Inorg. Chem. **2005**, *44*, 8602–8609

Wurster's Thiacrown Ethers: Synthesis, Properties, and Pt(II)-Coordination Chemistry

John W. Sibert,*,† Philip B. Forshee,† and Vincent Lynch‡

Department of Chemistry, The University of Texas at Dallas, Richardson, Texas 75083, and Department of Chemistry, The University of Texas, Austin, Texas 78712

Received July 6, 2005

Two isomeric redox-responsive azathiacrown ethers, based on *p*-phenylenediamine, have been synthesized in traditional crown (L_1) and crownophane (L_2) architectures. Each of these "Wurster's crowns" was designed to target the encapsulation of transition or heavy metal ions. The solid-state structures of these ligands show binding cavities defined by three exocyclic sulfur atoms and either a N donor atom (L_1) or the electron-rich π face of the phenylenediamine subunit (L_2). The ability of these ligands to form complexes with platinum(II) was investigated by various techniques including ^{1}H NMR spectroscopy, electrospray mass spectrometry, cyclic voltammetry, and single-crystal X-ray analysis. The traditional crown geometry proved to be better at forming stable endocyclic complexes with Pt(II) than the crownophane geometry. The square-planar Pt(II) crown complex includes direct bonding to the redox center (Pt1–N1 = 2.125 Å and Pt1–S_{av} = 2.278 Å) with concomitant polarization of the phenylenediamine moiety. This results in the crown complex oxidizing 916 mV more anodically than the free ligand. In contrast, modest shifts in the oxidation potential of the crownophane isomer indicate poor interaction between the redox center and complexed Pt(II) ion.

Introduction

Over the past two decades, considerable research has been conducted on electrochemically switchable ligand systems in which the binding of a guest alters the redox properties of the host or is modulated by the oxidation state of the host.[1] Recently, we and others have reported on novel families of redox-active macrocycles based on the three structural isomers of phenylenediamine.[2] Inspired by their structural relationship to the famed Wurster's reagent,[3] (*p*-TMPD), the trivial name "Wurster's crowns"[4] has been used to distinguish these macrocycles (Figure 1). The incorporation of the *p*-phenylenediamine moiety into a crown offers a distinct advantage over systems which rely purely on through-space electrostatic interactions between a redox center and guest. In Wurster's crowns, the macrocyclic N atom, critical to the electrochemical activity of the phenylenediamine moiety,

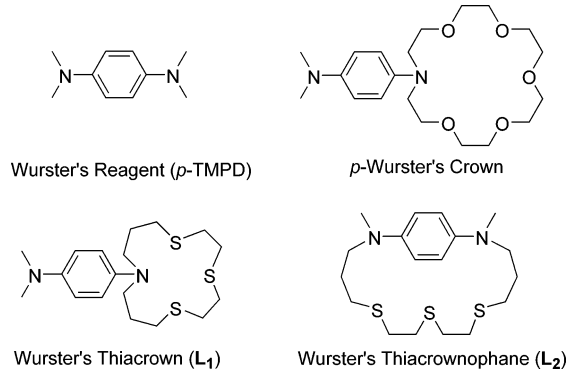

Figure 1. Wurster's reagent, the Wurster's crown analogue of 18-crown-6, and the two ligands from this study.

* To whom correspondence should be addressed. E-mail: sibertj@utdallas.edu.
† The University of Texas at Dallas.
‡ The University of Texas at Austin.

(1) (a) Kaifer, A. E.; Mendoza, S. In *Comprehensive Supramolecular Chemistry* Gokel, G. W., Atwood, J. L., Davies, J. E., MacNicol, D. D., Vögtle, F., Eds.; Pergamon: Oxford, 1996; Vol. 1, pp 701−732. (b) Boulas, P. L.; Gomez-Kaifer, M.; Echegoyen, L. *Angew. Chem., Int. Ed. Engl.* **1998**, *37*, 216−247.
(2) (a) Sibert, J. W.; Forshee, P. B. *Inorg. Chem.* **2002**, *41*, 5928−5930. (b) Sibert, J. W.; Seyer, D. J.; Hundt, G. R. *J. Supramol. Chem.* **2002**, *2*, 335−342. (c) Pearson, A. J.; Hwang, J. T. *Tetrahedron Lett.* **2001**, *42*, 3533−3536. (d) Pearson, A. J.; Hwang, J. T.; Ignatov, M. E. *Tetrahedron Lett.* **2001**, *42*, 3537−3540. (e) Pearson, A. J.; Hwang, J. T. *Tetrahedron Lett.* **2001**, *42*, 3541−3543. (f) Zhang, X.; Buchwald, S. L. *J. Org. Chem.* **2000**, *65*, 8027−8031. (g) Liu, X.; Eisenberg, A. H.; Stern, C. L.; Mirkin, C. A. *Inorg. Chem.* **2001**, *40*, 2940−2941. (h) Crochet, P.; Malval, J. P.; Lapouyade, R. *J. Chem. Soc., Chem. Commun.* **2000**, 289−290.
(3) Wurster, C. *Ber. Dtsch. Chem. Ges.* **1879**, *12*, 522−528.
(4) (a) Sibert, J. W. U.S. Patent 6,262,258, 2001. (b) Sibert, J. W. U.S. Patent 6,441,164, 2002.

10.1021/ic051125d CCC: $30.25
Published on Web 09/29/2005

serves to coordinate directly to a bound cationic guest. The result is a strong mutual interaction between the metal-ion guest and redox-active subunit in the form of a chemical bond. As such, these systems are well-suited for applications ranging from ion sensing to redox switching.

To date, all reported Wurster's crowns (and the vast majority of redox-active macrocycles in general) are redox-active analogues of crown ethers. As expected, these systems display affinities for Group I and Group II metal ions because of their predominance of hard oxygen-donor atoms. There are relatively few examples of redox-active macrocycles that are capable of forming complexes with transition and heavy metal ions.[5] We are interested in extending the Wurster's crown structural motif to new classes of redox-active macrocycles capable of coordinating softer metal ions. Thiacrown ethers have been extensively studied for their ability to bind a range of transition and heavy metal ions.[6] To increase the affinity of Wurster's crowns for these types of cationic guests we sought to incorporate an array of "S"-donor atoms within a Wurster's crown framework. The resultant Wurster's thiacrown ethers should not only display coordination chemistry akin to traditional thiacrown ethers, but, moreover, be electrochemically responsive to softer cations.

To develop general synthetic procedures to the Wurster's thiacrown ethers while gaining a fundamental understanding of their properties, we concentrated on two prototypical hosts, each providing a unique binding environment for cationic guests. The first ligand (**L_1**) represents a traditional crown structure with one N (from the phenylenediamine moiety) and three S-donor atoms arranged in a 14-membered ring. This molecular array should promote a strong communication pathway between the redox-active subunit and a bound cationic guest through the direct coordination of the endocyclic N atom. The second target ligand (**L_2**), a structural isomer of the first, formally a Wurster's thiacrownophane, contains a 13-membered polythioether bridge between the two N atoms of *p*-phenylenediamine. The resulting structure is a hybrid between a traditional crown and a cyclophane and is called a "crownophane". This ligand offers a binding pocket consisting of three S atoms as well as, potentially, the "soft" electron-rich π system of the redox center. The resultant topology uniquely provides a platform wherein cation$-\pi$ interactions could prove significant in complex formation and stability. Indeed, there is currently considerable interest in cation$-\pi$ interactions in biological systems.[7] Thus, we report here on the synthesis and properties of the first phenylenediamine-based thiacrown ethers and the subsequent study of their platinum(II) complexes.

(5) For examples, see: (a) LeDerf, F.; Mazari, M.; Mercier, N.; Levillain, E.; Richomme, P.; Becher, J.; Garín, J.; Orduna, J.; Gorgues, A.; Sallé, M. *J. Chem. Soc., Chem. Commun.* **1999**, 1417−1418. (b) Plenio, H.; Aberle, C.; Al Shihadeh, Y.; Lloris, J. M.; Martinez-Manez, R.; Pardo, T.; Soto, J. *Chem. Eur. J.* **2001**, *7*, 2848−2861. (c) Beer, P. D.; Smith, D. K. *J. Chem. Soc., Dalton Trans.* **1998**, 417−423.

(6) (a) Cooper, S. R.; Rawle, S. C. *Struct. Bonding* **1990**, *72*, 1−72. (b) Blake, A. J.; Schröder, M. *Adv. Inorg. Chem.* **1990**, *35*, 1.

(7) (a) Dougherty, D. A. *Science* **1996**, *271*, 163−168. (b) Hu, J.; Barbour, L.; Gokel, G. W. *J. Am. Chem. Soc.* **2002**, *124*, 10940−10941.

Experimental Section

Materials and Instrumentation. Unless otherwise noted, all reagents and solvents were acquired from commercial sources and used without further purification. All reactions were carried out under a dry argon atmosphere. For the synthesis of compound **L_2**, 4,7,10-trithiatridecane-1,13-di-*p*-toluenesulfonate was prepared by the methods of Baumann and co-workers,[8] and *N*,*N*′-dimethyl-1,4-phenylenediamine dihydrobromide was prepared via a modified procedure of Michaelis and co-workers.[9] $[Pt(C_2H_5CN)_4](SO_3CF_3)_2$ was synthesized in accordance with a previously published procedure.[10] ^{1}H and ^{13}C NMR spectra were recorded on a JEOL 270 MHz spectrometer. All experiments were conducted in deuterated chloroform ($CDCl_3$), dimethyl sulfoxide (DMSO-d_6), dichloromethane (CD_2Cl_2), or nitromethane (CD_3NO_2), and the chemical shifts were referenced to the residual hydrogen resonances of the solvent peak. Mass spectra were obtained from the Analytical Services Laboratories at Northwestern University. Electrospray (ES) mass spectra were measured using a Micromass Quatro II electrospray triple-quadrapole mass spectrometer. Electron impact (EI) mass spectra were measured using a Fisions VG 70−250 SE mass spectrometer. The elemental analyses were obtained from Atlantic Microlab, Inc.

Cyclic Voltammetry. Electrochemical experiments were conducted using a BAS CV-50W analyzer with a platinum microelectrode, a platinum-wire counter electrode, and an Ag/AgCl reference electrode. Potentials are cited versus the Ag/AgCl electrode. Cyclic voltammetry was performed in freshly distilled acetonitrile solutions containing 0.10 M electrochemical-grade tetraethylammonium tetrafluoroborate ($TEABF_4$). Solutions were purged with nitrogen prior to each experiment and run under an inert atmosphere.

Synthesis and Characterization. *N*-(4-nitrophenyl)-bis(3-hydroxypropyl)amine (1). A mixture of bis-3-hydroxypropylamine (4.15 g, 31.2 mmol) and 4-fluoronitrobenzene (2.00 g, 14.2 mmol) was stirred at 90 °C under an inert atmosphere for 16 h. When the reaction mixture cooled, it was loaded directly onto a silica gel column and eluted with a chloroform−methanol solution (9:1). Upon evaporation of the solvents, the product was obtained as a yellow solid. Yield: 2.87 g (80%). ^{1}H NMR (270 MHz, $CDCl_3$): δ 1.24 (s, 2H, O*H*), 1.87 (p, J = 5.9 Hz, 4H, $CH_2CH_2CH_2$), 3.57 (t, J = 7.2 Hz, 4H, CH_2N), 3.74 (t, J = 5.7 Hz, 4H, CH_2OH), 6.66 (d, J = 9.4 Hz, 2H, Ar-*H*), 8.09 (d, J = 9.4 Hz, 2H, Ar-*H*). ^{13}C NMR (DMSO-d_6): δ 30.3, 48.1, 58.6, 110.9, 126.5, 135.6, 153.3. MS (EI): m/z 254.1 $[M]^+$.

***N*-(4-nitrophenyl)-bis(3-(tosyloxy)propyl)amine (2).** A solution of *p*-toluenesulfonyl chloride (5.34 g, 28.0 mmol) in THF (20 mL) was added dropwise with stirring to a solution of **1** (2.85 g, 11.2 mmol) in THF (20 mL) and NaOH (1.51 g, 37.6 mmol) in water (20 mL). The mixture was stirred vigorously in an ice water bath for 6 h. Brine (20 mL) was added to the reaction mixture, and the organic layer was then isolated in a separatory funnel. Treatment of the organic layer with $MgSO_4$ and removal of the solvent by a rotary evaporator yielded the crude material that was further purified by recrystallization from methanol to give the desired product as a yellow crystalline solid. Yield: 4.20 g (67%). ^{1}H NMR (270 MHz, $CDCl_3$): δ 1.90 (p, J = 6.2 Hz, 4 H, $CH_2CH_2CH_2$), 2.43 (s, 6H, Ar−CH_3), 3.41 (t, J = 7.2 Hz, 4H, CH_2N), 4.05 (t, J = 5.7 Hz, 4H, CH_2OTs), 6.47 (d, J = 9.4 Hz, 2H, Ar-*H*), 7.35 (d, J = 7.9

(8) Baumann, T. F.; Reynolds, J. G.; Fox, G. A. *React. Funct. Polym.* **2000**, *44*, 111−120.

(9) Michaelis, L.; Schubert, M. P.; Granick, S. *J. Chem. Soc.* **1939**, *61*, 1981−1992.

(10) Kukushkin, V. Y.; Oskarsson, A.; Elding, L. I. *Inorg. Synth.* **1997**, *31*, 279−284.

Hz, 4H, Ar-*H*), 7.76 (d, $J = 8.4$ Hz, 4H, Ar-*H*), 7.98 (d, $J = 9.4$ Hz, 2H, Ar-*H*). ^{13}C NMR ($CDCl_3$): δ 21.7, 26.6, 47.4, 67.6, 110.6, 126.3, 127.9, 130.1, 132.7, 137.3, 145.4, 151.8. MS (EI): *m*/*z* 562.1 $[M]^+$.

***N*-(4-nitrophenyl)-1,4,7-trithia-11-azacyclotetradecane (3).** A solution of ditosylate **2** (6.86 g, 12.2 mmol) and 2-mercaptoethyl sulfide (2.09 g, 12.2 mmol) in DMF (125 mL) was added dropwise over 16 h with stirring to a mixture of DMF (450 mL) and Cs_2CO_3 (8.34 g, 25.6 mmol) at 60 °C. After the addition was complete, the mixture was stirred for an additional 20 h at 60 °C. Distillation of the DMF under reduced pressure yielded a crude solid that was partitioned between chloroform and water. The organic layer was collected, dried with $MgSO_4$, and removed via a rotary evaporator to yield a brown solid. The crude product was purified on a silica gel column eluted with chloroform. Yield: 2.34 g (52%). ^{1}H NMR (270 MHz, $CDCl_3$): δ 2.00 (p, $J = 7.4$ Hz, 4H, $CH_2CH_2CH_2$), 2.64 (t, $J = 7.1$ Hz, 4H, $NCH_2CH_2CH_2S$), 2.79 (s, 8H, CH_2S), 3.58 (t, $J = 7.4$ Hz, 4H, CH_2N), 6.60 (d, $J = 9.4$ Hz, 2H, Ar-*H*), 8.09 (d, $J = 9.4$ Hz, 2H, Ar-*H*). ^{13}C NMR ($CDCl_3$): δ 27.2, 29.6, 32.2, 32.3, 51.1, 110.8, 126.4, 137.4, 152.8. MS (EI): *m*/*z* 372.1 $[M]^+$.

***N*-(4-aminophenyl)-1,4,7-trithia-11-azacyclotetradecane (4).** A mixture of ethyl acetate (30 mL), 10% Pd/C (1.00 g, 0.94 mmol), and **3** (2.34 g, 6.30 mmol) was stirred under a H_2 atmosphere at room temperature for 24 h. The Pd/C was removed via filtration and rinsed with dichloromethane (3 × 25 mL). The organics were combined, and the solvent removed using a rotary evaporator to leave the desired product as a light brown oil. Yield: 2.13 g (99%). ^{1}H NMR (270 MHz, $CDCl_3$): δ 1.83 (p, $J = 7.7$ Hz, 4H, $CH_2CH_2CH_2$), 2.64 (t, $J = 7.3$ Hz, 4H, $NCH_2CH_2CH_2S$), 2.76 (m, 10H, CH_2S, NH_2), 3.17 (t, $J = 6.7$ Hz, 4H, CH_2N), 6.65 (m, 4H, Ar-*H*). ^{13}C NMR ($CDCl_3$): δ 28.8, 29.6, 31.6, 31.9, 52.2, 116.6, 118.2, 139.1, 142.9. MS (EI): *m*/*z* 342.1 $[M]^+$.

***N*-(*N*′,*N*′-dimethyl-4-aminophenyl)-1,4,7-trithia-11-azacyclotetradecane (L_1).** A mixture of $NaBH_4$ (0.90 g, 23.8 mmol) and **4** (2.04 g, 5.90 mmol) in EtOH (10 mL) was added dropwise over 5 min with stirring to a solution of 3 M H_2SO_4 (8.0 mL, 23.8 mmol) and 37% aqueous formaldehyde (2.20 mL, 23.8 mmol). The reaction mixture was stirred an additional 15 min at room temperature, at which point it was made strongly basic by the addition of 6 M NaOH. Dichloromethane (50 mL) was added to the reaction mixture, and the organic layer was collected and dried over Na_2SO_4. Filtration of the drying agent and removal of the solvent yielded a crude oil that was purified on a silica gel column eluted with chloroform. Yield: 1.92 g (87%). ^{1}H NMR (270 MHz, CD_2Cl_2): δ 1.83 (p, $J = 7.7$ Hz, 4H, $CH_2CH_2CH_2$), 2.63 (t, $J = 7.7$ Hz, 4H, $NCH_2CH_2CH_2S$), 2.74 (s, 8H, CH_2S), 2.81 (s, 6H, CH_3N), 3.29 (t, $J = 6.7$ Hz, 4H, CH_2N), 6.72 (m, 4H, Ar-*H*). ^{13}C NMR (CD_2Cl_2): δ 29.0, 29.5, 31.5, 31.8, 41.6, 52.3, 114.8, 117.4, 141.8, 144.7. HRMS (EI) calcd for $C_{18}H_{30}N_2S_3$ $[M]^+$ 370.1566. Found 370.1557.

2,16-Dimethyl-6,9,12-trithia-2,16-diaza-bicyclo[15.2.2]heneicosa-1(20),17(21),18-triene (L_2). A mixture of 4,7,10-trithiatridecane-1,13-di-*p*-toluenesulfonate (4.66 g, 8.10 mmol), *N*,*N*′-dimethyl-1,4-phenylenediamine dihydrobromide (2.40 g, 8.1 mmol), and Na_2CO_3 (6.83 g, 64.4 mmol) was stirred in refluxing acetonitrile (350 mL) for 3 days. The solvent was removed under reduced pressure to leave a dark solid that was partitioned between chloroform and water. The organic layer was dried with Na_2SO_4, and following filtration of the drying agent and solvent removal, the dark brown oil was purified via column chromatography (silica gel eluted with chloroform). Yield: 470 mg (16%). ^{1}H NMR (270 MHz, CD_2Cl_2): δ 1.73 (p, $J = 6.9$ Hz, 4H, $CH_2CH_2CH_2$), 2.48 (t, $J = 7.2$ Hz, 4H, $NCH_2CH_2CH_2S$), 2.59 (s, 8H, CH_2S), 2.81 (s, 6H, CH_3N), 3.36 (t, $J = 6.9$ Hz, 4H, CH_2N), 6.77 (s, 4H, Ar-*H*). ^{13}C NMR (CD_2Cl_2): δ 26.0, 29.8, 32.3, 32.8, 39.1, 51.6, 115.3, 141.7; HRMS (EI) calcd for $C_{18}H_{30}N_2S_3$ $[M]^+$ 370.1566. Found 370.1560.

$[Pt(L_1)](SO_3CF_3)_2$. In an argon-filled glovebox, separate dichloromethane solutions (ca. 3 mL total volume) of L_2 (30 mg, 81 mmol) and $[Pt(C_2H_5CN)_4](SO_3CF_3)_2$ (58 mg, 81 mmol) were combined to produce a deep yellow reaction mixture. The solution was then allowed to evaporate in the inert atmosphere leaving a crude off-white solid. Analytical samples were prepared through crystallization by dissolving the crude solid in nitromethane and adding diethyl ether by vapor diffusion at room temperature in ambient air. The supernatant was decanted and the remnant crystals washed with diethyl ether and dried under reduced pressure. Yield: 50 mg (71%). ^{1}H NMR (270 MHz, CD_3NO_2): δ 2.27 (br, 2H, $CH_2CH_2CH_2$), 2.70 (br, 2H, $CH_2CH_2CH_2$), 3.00 (s, 6H, CH_3N), 3.25−4.16 (m, 16H, CH_2N, CH_2S), 6.80 (d, $J = 8.9$ Hz, 2H, Ar-*H*), 7.89 (d, $J = 8.9$ Hz, 2H, Ar-*H*). Anal. Calcd for $C_{20}H_{30}F_6N_2O_6PtS_5$: C, 27.81; H, 3.50; N, 3.24. Found: C, 27.74; H, 3.52; N, 3.28. ESI-MS: *m*/*z* 714.1(100) $[L_1 + Pt^{2+} + OTf]^+$, 601.1(35) $[L_1 + Pt^{2+} + Cl^-]^+$, 564.3(29) $[L_1 + Pt^{2+} - H^+]^+$, 282.7(95) $[L_1 + Pt^{2+}]^{2+}$. Despite a preliminary structure that revealed an endocyclic complex, attempts to obtain an acceptable X-ray crystal structure of this compound were unsuccessful because of data that could not be fully refined. To obtain a sample for X-ray analysis, the triflate anions were exchanged for hexafluorophosphate using the following procedure. Excess NH_4PF_6 was added to a small sample of $[Pt(L_1)](SO_3CF_3)_2$ in H_2O, heated to reflux. When the mixture cooled, a creamy white solid was collected via filtration and dried in vacuo. X-ray quality crystals were then prepared from the slow diffusion of ethyl ether into a concentrated nitromethane solution of $[Pt(L_1)](PF_6)_2$. Anal. Calcd for $C_{18}H_{30}F_{12}N_2P_2PtS_3$: C, 25.27; H, 3.53; N, 3.27. Found: C, 25.25; H, 3.30; N, 3.21. This complex gave an identical ^{1}H NMR spectrum to that of the corresponding triflate complex.

Crystal Growth and Structure Determination. Crystal structures for compounds L_1, L_2, and $[Pt(L_1)](PF_6)_2$ have been determined. Data for the samples were collected on a Nonius Kappa CCD diffractometer using a graphite monochromator with Mo Kα radiation ($\alpha = 0.71073$ Å). The data for L_2 were collected at 173 K, while the data for L_1 and $[Pt(L_1)](PF_6)_2$ were collected at 153 K using an Oxford Cryostream low-temperature device. In all three structures, data reduction was performed using DENZO-SMN.[11] The structures were solved by direct methods using SIR97[12] and refined by full-matrix least-squares on F^2 with anisotropic displacement parameters for the non-H atoms using SHELXL-97.[13] In each case, the hydrogen atoms on carbon were calculated in ideal positions with isotropic displacement parameters set to $1.2U_{eq}$ of the attached atom ($1.5U_{eq}$ for methyl hydrogen atoms). Neutral atom-scattering factors and values used to calculate the linear absorption coefficient are from the International Tables for X-ray Crystallography (1992).[14] Definitions used for calculating $R(F)$, R_w

(11) For DENZO-SMN, see: Otwinowski, Z.; Minor, W. In *Methods in Enzymology, Vol. 276: Macromolecular Crystallography*; Carter, C. W., Jr., Sweet, R. M., Eds.; Academic Press: New York, 1997; Part A, pp 307−326.

(12) For SIR97, a program for crystal structure solution, see: Altomare, A.; Burla, M. C.; Camalli, M.; Cascarano, G. L.; Giacovazzo, C.; Guagliardi, A.; Moliterni, A. G. G.; Polidori, G.; Spagna, R. *J. Appl. Crystallogr.* **1999**, *32*, 115−119.

(13) Sheldrick, G. M. *SHELXL97. Program for the Refinement of Crystal Structures*; University of Göttingen: Göttingen, Germany, 1994.

(14) *International Tables for X-ray Crystallography*; Wilson, A. J. C., Ed.; Kluwer Academic Press: Boston, 1992; Vol. C, Tables 4.2.6.8 and 6.1.1.4.

Table 1. Summary of Crystallographic Data for Compounds $\mathbf{L_1}$, $\mathbf{L_2}$, and $[Pt(\mathbf{L_1})](PF_6)_2 \cdot 0.5CH_3NO_2$

	$\mathbf{L_1}$	$\mathbf{L_2}$	$[Pt(\mathbf{L_1})](PF_6)_2 \cdot 0.5CH_3NO_2$
empirical formula	$C_{18}H_{30}N_2S_3$	$C_{18}H_{30}N_2S_3$	$C_{18.5}H_{31.5}F_{12}N_{2.5}OP_2PtS_3$
mol wt	370.62	370.62	886.17
cryst syst	triclinic	triclinic	orthorhombic
space group	$P\bar{1}$	$P\bar{1}$	*Pnma*
a (Å)	5.8862(1)	8.3850(3)	22.2663(2)
b (Å)	12.0606(3)	11.8510(4)	33.2258(2)
c (Å)	14.9082(4)	19.9250(7)	15.2499(1)
α (deg)	112.330(1)	90.188(2)	90
β (deg)	90.565(1)	101.3740(17)	90
γ (deg)	90.445(1)	90.847(2)	90
V (Å^3)	978.86(4)	1940.82(12)	11282.12(14)
Z	2	4	16
temp (K)	153(2)	173(2)	153(2)
ρ_{calcd} (Mg/m^{-3})	1.257	1.268	2.087
μ (mm^{-1})	0.380	0.384	5.410
GOF on F^2	0.0997	1.378	1.398
final R indices [$I > 2\sigma(I)$]			
R	0.0416	0.0704	0.0472
R_w	0.0864	0.1740	0.1132
R indices (all data)			
R	0.0909	0.0769	0.0738
R_w	0.1018	0.1772	0.1203

(F^2) and the goodness of fit, S, are as referenced.[15] Details of crystal data, data collection and structure refinement are listed in Table 1. Selected bond lengths and angles are listed in Table 2.

Crystals of $\mathbf{L_1}$ grew as clusters of colorless lathes by slow evaporation from hexane and dichloromethane. The data crystal was cut from a cluster of crystals and had approximate dimensions of 0.28 × 0.12 × 0.09 mm. A total of 560 frames of data were collected using ω scans with a scan range of 1° and a counting time of 103 s per frame. The function, $\sum w(|F_o|^2 - |F_c|^2)^2$, was minimized, where $w = 1/[(\sigma(F_o))^2 + (0.0436P)^2 + (0.646P)]$ and $P = (|F_o|^2 + 2|F_c|^2)/3$. $R_w(F^2)$ refined to 0.102, with $R(F)$ equal to 0.0416 and a goodness of fit of $S = 1.00$. The data were checked for secondary extinction effects but no correction was needed.

Crystals of $\mathbf{L_2}$ grew as pale-yellow needles by slow evaporation from dichloromethane. A total of 322 frames of data were collected using ω scans with a scan range of 1.4° and a counting time of 105 s per frame. The crystal has monoclinic metric symmetry. However, the diffraction symmetry is triclinic. The R_{int} for a monoclinic data set is 27.8% for 9339 unique reflections out of 12649 total measured reflections. The R_{int} for a triclinic data set is 3.0% for 4169 unique reflections. In the triclinic setting, $Z' = 2$. The two molecules are related by a pseudo 2-fold screw-rotation axis with approximate symmetry $1 - x$, $1/2 + y$, $1/2 - z$. The refinement showed some of the typical warning signs of twinning. In particular, there were many reflections with large, positive $\Delta(|F_o|^2 - |F_c|^2)$ values. The utility ROTAX[16] in the program WinGX[17] was used to look for possible twins. ROTAX suggested a possible twin with twin law −100/010/0,0,−1 about the direct axis 010 direction. Refinement resulted in a twin fraction of 0.205(2). The use of the twin refinement resulted in a lowering of R_w from 0.276 to 0.182 and R from 0.139 to 0.0731. The function, $\sum w(|F_o|^2 - |F_c|^2)^2$, was minimized, where $w = 1/[(\sigma(F_o))^2 + (0.0344P)^2 + (4.0711P)]$ and $P = (|F_o|^2 + 2|F_c|^2)/3$. $R_w(F^2)$ refined to 0.177, with $R(F)$ equal to 0.0704 and a goodness of fit of 1.38. The data were corrected for secondary extinction effects. The correction takes the form $F_{corr} = kF_c/[1 + (4.5(12) \times 10^{-6})F_c^2\lambda^3/(\sin 2\theta)]^{0.25}$, where k is the overall scale factor.

Table 2. Selected Bond Lengths (Å) and Bond Angles (deg) of Structures $\mathbf{L_1}$, $\mathbf{L_2}$, and One of the Two Structurally Similar Complexes in $[Pt(\mathbf{L_1})](PF_6)_2$

		$\mathbf{L_1}$	
C1−N1	1.462(2)	C3−S1	1.811(2)
C10−N1	1.470(2)	C4−S1	1.810(2)
C11−N1	1.422(2)	C5−S2	1.809(2)
C14−N2	1.410(2)	C6−S2	1.813(2)
C17−N2	1.456(2)	C7−S3	1.811(2)
C18−N2	1.452(3)	C8−S3	1.810(2)
C3−S1−C4	97.99(9)	C1−N1−C11	117.14(16)
C5−S2−C6	101.04(10)	C14−N2−C17	116.74(17)
C7−S3−C8	102.50(10)	C17−N2−C18	113.78(17)
C1−N1−C10	114.25(15)	C14−N2−C18	116.83(17)
C10−N1−C11	116.66(15)		
		$\mathbf{L_2}$	
C1−N1	1.413(4)	C9−S1	1.826(4)
C16−N1	1.458(4)	C10−S1	1.810(4)
C18−N1	1.454(5)	C11−S2	1.827(4)
C4−N2	1.396(4)	C12−S2	1.804(4)
C7−N2	1.454(5)	C13−S3	1.830(4)
C17−N2	1.455(5)	C14−S3	1.823(4)
C9−S1−C10	102.81(17)	C1−N1−C18	117.8(3)
C11−S2−C12	100.01(17)	C4−N2−C7	119.4(3)
C13−S3−C14	98.55(17)	C7−N2−C17	116.2(3)
C1−N1−C16	119.0(3)	C4−N2−C17	117.9(3)
C16−N1−C18	114.0(3)		
		$[Pt(\mathbf{L_1})](PF_6)_2$	
C1−N1	1.539(8)	C5−S2	1.824(7)
C10−N1	1.505(8)	C6−S2	1.818(7)
C11−N1	1.444(8)	C7−S3	1.804(7)
C14−N2	1.341(9)	C8−S3	1.814(7)
C17−N2	1.490(12)	Pt1−S1	2.2983(18)
C18−N2	1.416(11)	Pt1−S2	2.2385(18)
C3−S1	1.798(8)	Pt1−S3	2.2961(18)
C4−S1	1.796(7)	Pt1−N1	2.125(5)
C3−S1−C4	103.2(4)	C17−N2−C18	115.6(7)
C5−S2−C6	105.9(3)	C14−N2−C18	121.5(8)
C7−S3−C8	103.8(3)	S1−Pt1−N1	91.23(15)
C1−N1−C10	106.4(5)	S1−Pt1−S2	88.07(6)
C10−N1−C11	107.3(5)	S2−Pt1−S3	87.74(7)
C1−N1−C11	111.5(5)	S3−Pt1−N1	92.66(15)
C14−N2−C17	118.4(7)		

(15) $R_w(F^2) = \{\sum w(|F_o|^2 - |F_c|^2)^2/\sum w(|F_o|)^4\}^{1/2}$, where w is the weight given each reflection. $R(F) = \sum(|F_o| - |F_c|)/\sum|F_o|\}$ for reflections with $F_o > 4(\sigma(F_o))$. $S = [\sum w(|F_o|^2 - |F_c|^2)^2/(n - p)]^{1/2}$, where n is the number of reflections and p is the number of refined parameters.

(16) For ROTAX, see: Cooper, R. I.; Gould, R. O.; Parsons, S.; Watkin, D. J. *J. Applied Cryst.* **2002**, *35*, 168−174.

(17) For WinGX, see: Farrugia, L. J. *J. Applied Cryst.* **1999**, *32*, 837−838.

Scheme 1. Synthetic Scheme for Ligand $\mathbf{L_1}$

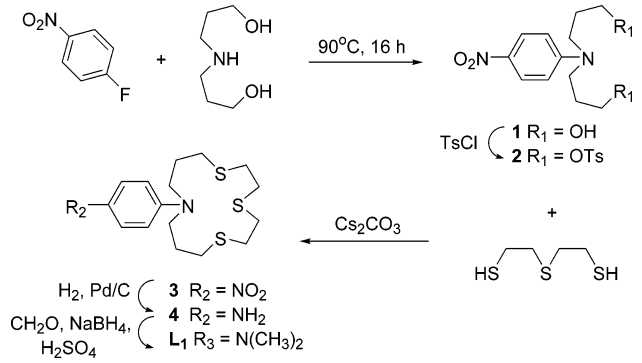

Scheme 2. Synthetic Scheme for Ligand $\mathbf{L_2}$

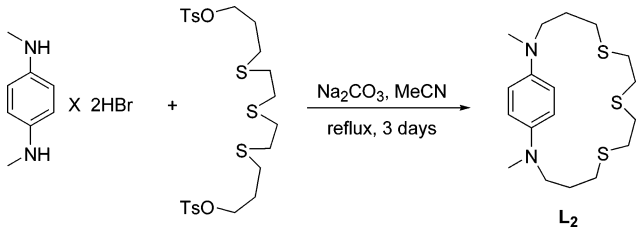

Crystals of $[Pt(\mathbf{L_1})](PF_6)_2 \cdot 0.5CH_3NO_2$ grew as large colorless prisms by the vapor diffusion of ethyl ether into a nitromethane solution. The data crystal was cut from a larger crystal and had approximate dimensions of 0.24 × 0.24 × 0.16 mm. A total of 448 frames of data were collected using ω scans with a scan range of 0.9° and a counting time of 118 s per frame. The unit cell consists of a layer containing the anions and nitromethane solvent molecules sandwiched by two layers of the Pt crown complex. This sandwich forms around a crystallographic mirror plane at $y = 1/4$. Four half-weighted anions lie on this mirror plane containing the phosphorus atoms P1b, P1c, P1d, and P1e. Except for the anion with P1c, the hexafluorophosphate anions are reasonably well behaved. The anion consisting of P1c, F1c, F2c, F3c, F4c, and F5c was found to be disordered. F1c was the sole F atom not lying on the crystallographic mirror plane. The disorder could be modeled by a 45° rotation about the F1c−P1c bond. The site occupancy factor for the disordered F atoms were determined by assigning the variable x to the site occupancy of one set of four F atoms (F2c, F3c, F4c, and F5c) and $(1 - x)$ to the second set of F atoms (F2ca, F3ca, F4ca, and F5ca). The site occupancy factor, x, refined to 64(2)% using a common isotropic displacement parameter for the eight F atoms. The geometry of this anion and the anions lying on the crystallographic mirror was restrained to be approximately equivalent. In addition, the anisotropic displacement parameters were restrained to be approximately isotropic. The $\sum w(|F_o|^2 - |F_c|^2)^2$ function was minimized, where $w = 1/[(\sigma(F_o))^2 + (0.044P)^2]$ and $P = (|F_o|^2 + 2|F_c|^2)/3$. $R_w(F^2)$ refined to 0.120 with $R(F)$ equal to 0.0472 and a goodness of fit of 1.60. The data were checked for secondary extinction effects, but no correction was necessary.

Results and Discussion

Synthesis. The target ligands, $\mathbf{L_1}$ and $\mathbf{L_2}$, were prepared using two distinct reaction sequences (Schemes 1 and 2). Each synthetic procedure is likely to be sufficiently general to allow for the preparation of a myriad of Wurster's thiacrown ethers in either the crownophane or traditional crown architecture. Ligand $\mathbf{L_1}$ was prepared in five steps beginning with the selective N-arylation of the commercially available bis(3-hydroxypropyl)amine via nucleophilic aromatic substitution on 4-fluoronitrobenzene. Following tosylation of the resultant diol, cyclization with 2-mercaptoethyl sulfide produced **3** in a 50% yield. Hydrogenation and methylation gave the final product in an overall yield of 25%.

Ligand $\mathbf{L_2}$ was formed in typical yields of 15−20% from the cyclocondensation of *N*,*N*′-dimethyl-1,4-phenylenediamine dihydrobromide with 4,7,10-trithiatridecane-1,13-di-*p*-toluenesulfonate in the presence of sodium carbonate. A decrease in the concentration of reactants, an increase in the reaction time, or a change in the alkali-metal carbonate base did not improve the efficiency of the reaction significantly.

Coordination Chemistry. The presence of thioether functionalities should endow ligands $\mathbf{L_1}$ and $\mathbf{L_2}$ with the ability to coordinate softer cations. As such, we focused our efforts on the encapsulation of Pt(II). In addition, this provides the opportunity to compare complex properties to existing data on a number of structurally related, but not redox-active Pt(II)−thia- and azathiacrown ether complexes[18] to gauge the impact of the redox center on the coordination chemistry of the ligands. The platinum(II) complex of $\mathbf{L_1}$ was prepared by combination of equimolar dichloromethane solutions of $\mathbf{L_1}$ and $[Pt(C_2H_5CN)_4](SO_3CF_3)_2$ at room temperature in an argon-filled glovebox. The reaction mixture rapidly darkened to a deep yellow-gold color. Upon evaporation of the solvent in an argon atmosphere, the crude $[Pt(\mathbf{L_1})](SO_3CF_3)_2$ was crystallized by the vapor diffusion of ethyl ether into a nitromethane solution. The pale yellow crystals that resulted were suitable for elemental analysis but did not allow for a fully refined X-ray structure to be obtained. In an effort to grow crystals suitable for X-ray analysis, the triflate anions were exchanged for hexafluorophosphate anions. Metathesis was accomplished by the addition of excess NH_4PF_6 to an aqueous solution of $[Pt(\mathbf{L_1})](SO_3CF_3)_2$ heated to reflux. When the mixture cooled to room temperature, a creamy white solid formed that was separated from the solution by filtration. The solid was then dissolved in a minimal quantity of nitromethane and diethyl ether was diffused into the solution rendering X-ray quality crystals of $[Pt(\mathbf{L_1})](PF_6)_2$.

In a similar fashion, the combination of equimolar solutions of $\mathbf{L_2}$ and $[Pt(C_2H_5CN)_4](SO_3CF_3)_2$ resulted in a near instantaneous darkening of the mixture. Upon evaporation of the dichloromethane solvent, attempts to purify the crude complex by crystallization proved unsuccessful. Of particular note and in contrast to $[Pt(\mathbf{L_1})](SO_3CF_3)_2$, solutions of the putative $[Pt(\mathbf{L_2})](SO_3CF_3)_2$ complex darken substantially and

(18) For examples, see: (a) Waknine, D.; Heeg, M. J.; Endicott, J. F.; Ochrymowycz, L. A. *Inorg. Chem.* **1991**, *30*, 3691−3700. (b) Watzky, M. A.; Waknine, D.; Heeg, M. J.; Endicott, J. F.; Ochrymowycz, L. A. *Inorg. Chem.* **1993**, *32*, 4882−4888. (c) Blake, A. J.; Holder, A. J.; Reid, G.; Schröder, M. *J. Chem. Soc., Dalton Trans.* **1994**, 627−631. (d) Chandrasekhar, S.; Waltz, W. L.; Prasad, L.; Quail, J. W. *Can. J. Chem.* **1997**, *75*, 1363−1374. (e) Chak, B.; McAuley, A.; Whitcombe, T. W. *Inorg. Chim. Acta* **1996**, 349−360. (f) Grant, G. J.; Chen, W.; Goforth, A M.; Baucom, C. L.; Patel, K.; Repovic, P.; VanDerveer, D. G.; Pennington, W. T. *Eur. J. Inorg. Chem.* **2005**, 479−485. (g) Grant, G. J.; Goforth, A M.; VanDerveer, D. G.; Pennington, W. T. *Inorg. Chim. Acta* **2004**, 2107−2114. (h) Grant, G. J.; Spangler, N. J.; Setzer, W. N.; VanDerveer, D. G.; Mehne, L. F. *Inorg. Chim. Acta* **1996**, 30−41.

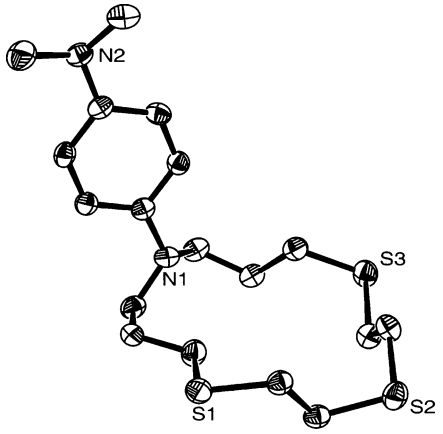

Figure 2. X-ray structure of $\mathbf{L_1}$ (H atoms omitted for clarity). Thermal ellipsoids are plotted at the 50% level.

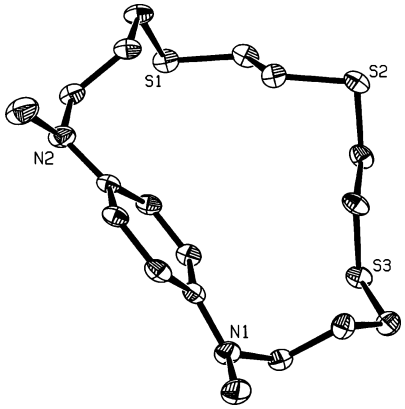

Figure 3. X-ray structure of $\mathbf{L_2}$ (H atoms omitted for clarity). Thermal ellipsoids are plotted at the 50% level.

take on a "Wurster's blue" color when exposed to ambient air. This behavior is characteristic of uncomplexed Wurster's crowns and is attributed to oxidation of the redox center to the radical cation state. Importantly, it suggests either that no complex was formed or the Pt(II) cation has little or no interaction with the redox-active moiety in its complex with $\mathbf{L_2}$. Analysis of the crude reaction mixture by both variable-temperature ^{1}H NMR spectroscopy (−20 to 80 °C) and mass spectrometry proved inconclusive as to the nature of the complex(es) formed (e.g., endocyclic vs exocyclic) with the former technique giving broad unresolved spectral features over the temperature range studied. However, electrochemical analysis suggested the probable formation of exocyclic structures (vide infra) with weak to no participation by the redox center in the coordination of the Pt(II) cation.

Solid State Structures. ORTEP representations of ligands $\mathbf{L_1}$ and $\mathbf{L_2}$ and [Pt($\mathbf{L_1}$)](PF$_6$)$_2$ are shown in Figures 2, 3, and 4, respectively. Crystal data and details of data collection and refinements are summarized in Table 1. Selected bond lengths and angles for the structures are presented in Table 2.

The solid-state structures of $\mathbf{L_1}$ and $\mathbf{L_2}$ demonstrate significant sp^2 hybridization about both the macrocyclic and dimethylamino N atoms (C−N−C$_{av}$ 115.90° and 117.38° for $\mathbf{L_1}$ and $\mathbf{L_2}$, respectively), allowing for both N atoms to function as π donors to the phenyl ring. The crownophane architecture necessitates the inclusion of both phenylenediamine "N" atoms within the macrocyclic framework, creating a 19-membered macrocycle for ligand $\mathbf{L_2}$ that is significantly larger than the 14-membered macrocyclic ring for the traditional crown isomer $\mathbf{L_1}$. The methyl groups in the crownophane $\mathbf{L_2}$ are cis with respect to the phenyl unit. Within the crown region, both ligands exhibit an exodentate orientation of the sulfur atoms. This is typical of thiacrown ethers and is attributed to the preference of C−S bonds to adopt gauche conformations. For example, the X-ray structure of [12]aneS$_4$ shows all gauche C−S bonds and anti C−C bonds, resulting in the positioning of the four S atoms at the corners of a box-shaped macrocycle.[19] Indeed, of the six C−S bonds in both $\mathbf{L_1}$ and $\mathbf{L_2}$, five are gauche. In fact, both structures can be viewed as quite similar to that of [12]aneS$_4$ with the redox center formally replacing one of the four S atoms.

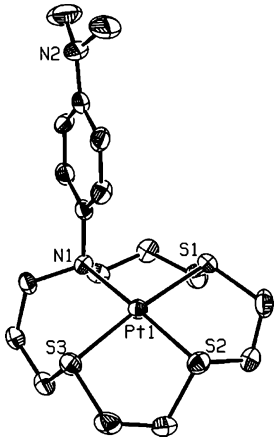

Figure 4. One of the two structurally similar complexes present in the X-ray structure of [Pt($\mathbf{L_1}$)](PF$_6$)$_2$ (H atoms and PF$_6^-$ anions omitted for clarity). Thermal ellipsoids are plotted at the 50% level.

Two distinct complexes of [Pt($\mathbf{L_1}$)](PF$_6$)$_2$ were present in the single crystal, although, in terms of the complexed cation, the geometric parameters are nearly identical with each unequivocally showing the endocyclic encapsulation of the platinum(II) cation. (It is worth noting that a preliminary structure of the triflate complex, [Pt($\mathbf{L_1}$)](SO$_3$CF$_3$)$_2$, showed essentially the same complex cation geometry.) In sharp contrast to the structure of the corresponding free macrocyclic host, $\mathbf{L_1}$, all three of the sulfur atoms have assumed an endocyclic orientation creating a binding pocket for the platinum(II) cation inside of the macrocyclic cavity. The dramatic reorientation of the macrocyclic structure is apparent through a comparison of the torsional angles about the C−S bonds. In the complex, only two of the six C−S bonds remain gauche. The three sulfur and one nitrogen donor atom array form a near square-planar geometry about the platinum atom that is disposed 0.10 Å above the plane of donor atoms. As expected, this arrangement is similar to that for platinum(II) complexes of [14]aneS$_4$ and [14]aneN$_4$. The average Pt−S distances in [Pt($\mathbf{L_1}$)](PF$_6$)$_2$ (Pt1−S = 2.278 Å) are consistent with those reported for [Pt([14]aneS$_4$)](ClO$_4$)$_2$ (2.288 Å),[18a] [Pt([12]aneS$_4$)](Cl)$_2$·H$_2$O (2.293 Å),[18b] and [Pt-

(19) Wolfe, R. E.; Hartman, J. R.; Storey, J. M.; Foxman, B. M.; Cooper, S. R. *J. Am. Chem. Soc.* **1987**, *109*, 4328−4335.

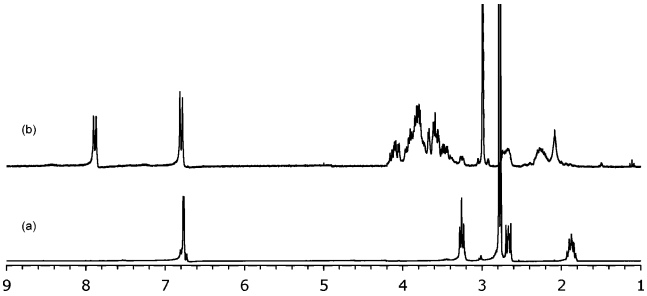

Figure 5. ^{1}H NMR spectra of (a) $\mathbf{L_1}$ and (b) [Pt($\mathbf{L_1}$)](SO_3CF_3)$_2$ in CD_3NO_2.

([12]aneS_4)][PF_6]$_2$ (2.282 Å)[18c] with the shortest Pt−S bond trans to the Pt−N bond. Similarly, the Pt−N distance in [Pt($\mathbf{L_1}$)](PF_6)$_2$ (Pt1−N1 = 2.125(5) Å) is close to that of [Pt([14]aneN_4)](ClO_4)$_2$ (av 2.053 Å),[18d] despite the aryl substituent in $\mathbf{L_1}$. Undoubtedly, the presence of the *para*-dimethylamino group greatly increases the donor ability of the macrocyclic N atom in $\mathbf{L_1}$. Another characteristic feature observed upon complexation of the Wurster's thiacrown is the near 90° rotation of the phenyl ring with respect to the plane of the crown. This behavior results in a rehybridization of the macrocyclic nitrogen from near sp^2 in the uncomplexed form to sp^3 in the metal complex, greatly reducing the orbital overlap of the macrocyclic N atom with the π system. The increased Lewis basicity reflects a macrocyclic N atom that is more "amine-like" (σ donor) and less "aniline-like" (π donor) in the complex which allows for a stronger mutual interaction between it and the bound metal guest. In $\mathbf{L_1}$, the macrocyclic C−N−C_{av} is 116.02°. Upon complexation of platinum, the C−N−C_{av} bond angle has been reduced to 108.4°, very near the theoretical 109.5° angle representing complete pyramidalization of the nitrogen atom. The distal dimethylamino group adopts a more planar geometry (C−N−C_{av} bond angle = 118.5°) versus that in the free ligand to compensate for the decrease in electron density at the macrocyclic N atom in the complex.

^{1}H NMR Spectroscopy. Chemical shifts and splitting patterns for $\mathbf{L_1}$ and $\mathbf{L_2}$ were as expected for hybrid structures of *p*-TMPD and thiacrown ethers. In contrast to the solid-state structure of $\mathbf{L_2}$, which shows the methyl groups in a cis geometry, the presence of a single aromatic resonance in $\mathbf{L_2}$ indicates rapid rotation about the C_{aryl}−N bonds so that the four aromatic H atoms are in identical chemical environments. Unlike *p*-TMPD, the asymmetrically substituted phenylenediamine in $\mathbf{L_1}$ causes two sets of unique aromatic H atoms. However, their similar chemical environments preclude the appearance of discrete resonances, instead producing a closely spaced multiplet pattern centered at 6.72 ppm. Thus, the formal replacement of two methyl groups of *p*-TMPD with a crown functionality does not significantly alter the structure of the phenylenediamine moiety. This is significant as the expected electrochemical properties of Wurster's thiacrown ethers should then be comparable to that of *p*-TMPD, a key premise to this study.

The ^{1}H NMR spectrum of [Pt($\mathbf{L_1}$)](SO_3CF_3)$_2$ recorded at 298 K in CD_3NO_2 (Figure 5) shows a complex second-order splitting pattern in the range δ 3.25−4.18 ppm because of the methylene resonances next to the heteroatoms of the macrocycle. Similar spectral features have been noted in a variety of simple thiacrown Pt(II) complexes in the literature.[18a,18c] Further, the two sets of aromatic H atoms are no longer alike as the Pt(II) ion polarizes the phenyl ring. The polarization has contributions from the close proximity of the Pt(II) cation (electrostatic) and the rehybridization of the macrocyclic N atom (sp^2 to sp^3). This results in an AA′BB′ pattern characteristic of an asymmetrically substituted phenyl ring in which the two substituents have substantially different electronic demands or electronegativities. The two aromatic H atoms proximal to the ligated macrocyclic N atom are shifted downfield clearly indicating the strong interaction between the macrocyclic amine and the Pt(II) ion in solution. A downfield shift is also observed for the protons of the methyl group ($\mathbf{L_1}$, 2.83 ppm; [Pt($\mathbf{L_1}$)](SO_3CF_3)$_2$, 3.02 ppm), revealing that the binding event is sensed across the entire redox center. In contrast, the ^{1}H NMR spectrum of the putative [Pt($\mathbf{L_2}$)](SO_3CF_3)$_2$ complex measured under the same conditions has a series of very broad uninterpretable resonances that changed little over a 100 °C temperature range (−20 to 80 °C).

Electrochemistry. The electrochemical properties of ligands $\mathbf{L_1}$ and $\mathbf{L_2}$, along with those of their Pt(II) complexes, were studied by cyclic voltammetry. As shown in Figure 6a, both $\mathbf{L_1}$ and $\mathbf{L_2}$ display two reversible oxidations with the first corresponding to a delocalized radical cation and the second to a quinoid-like dication. This electrochemical behavior mimics that of *p*-TMPD and demonstrates that formal replacement of the two methyl groups of *p*-TMPD with a crown has no effect on the gross electrochemical features of the parent redox-active moiety.

Interestingly, the first oxidation of $\mathbf{L_2}$ is 19 mV more cathodic than that of $\mathbf{L_1}$. The more facile oxidation of $\mathbf{L_2}$ likely stems from the favorable orientation of the polythioether subunit with respect to the phenyl ring. Upon oxidation, the positive charge of the delocalized radical cation can be stabilized by interactions with the lone pairs of the sulfur atoms. This intramolecular stabilization is not possible for the traditional crown structure of $\mathbf{L_1}$.

As has been shown for a variety of redox-active macrocycles, the binding of a metal cation generally results in anodic shifts in the oxidation potentials of the ligands because of the electrostatic interactions associated with two cations in close proximity and "through-bond" inductive effects. Samples of $\mathbf{L_1}$, $\mathbf{L_2}$, and their corresponding preformed metal complexes were dissolved in acetonitrile solutions containing 0.1 M $TEABF_4$. In the case of $\mathbf{L_2}$, the crude product formed from the reaction with [Pt(C_2H_5CN)$_4$](SO_3CF_3)$_2$ was used without purification. As shown in Figure 6b, the complexation of Pt(II) by $\mathbf{L_1}$ results in an anodic shift of 916 mV accompanied by a loss of reversibility. The magnitude of the electrochemical shift indicates a strong interaction between the host and metal-ion guest, suggesting the solution-phase structure of [Pt($\mathbf{L_1}$)](SO_3CF_3)$_2$ is very similar to that determined in the solid phase through X-ray analysis. In contrast, Figure 6c shows an overlay of the cyclic voltammograms for $\mathbf{L_2}$ and [Pt($\mathbf{L_2}$)](SO_3CF_3)$_2$. Upon com-

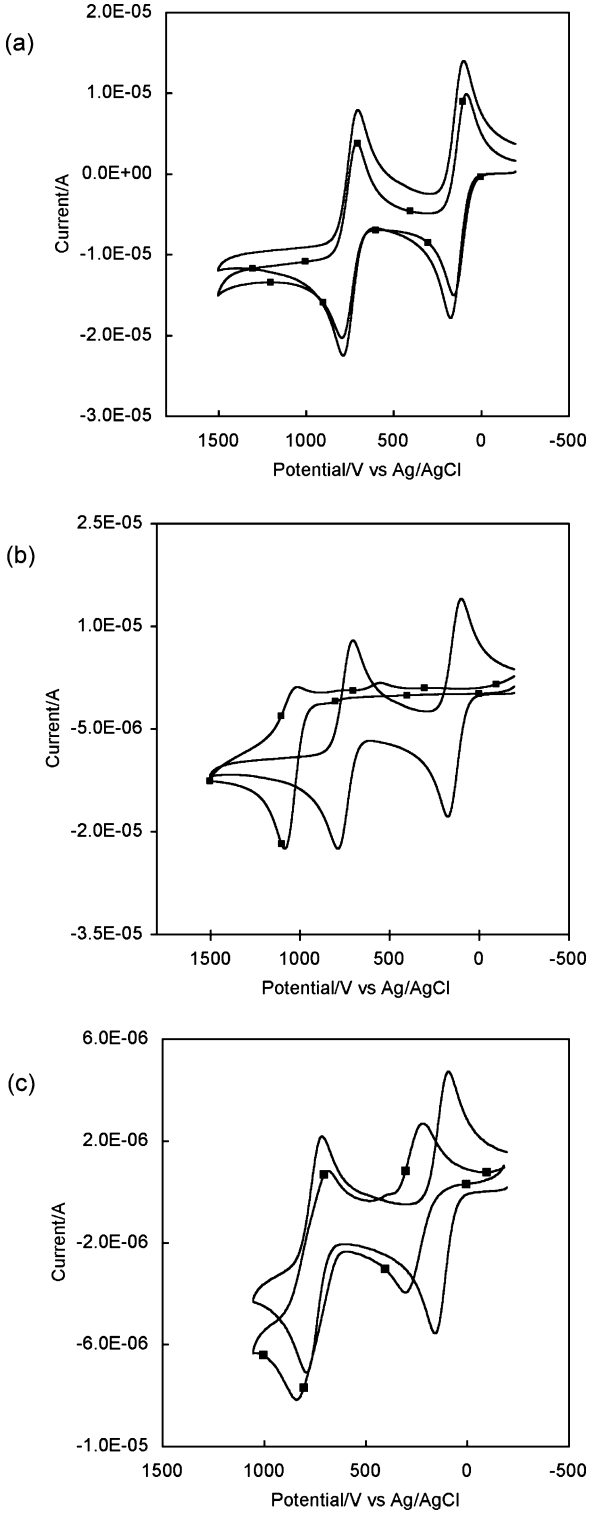

Figure 6. Cyclic voltammograms of (a) $\mathbf{L_1}$ (—) and $\mathbf{L_2}$ (—■—), (b) $\mathbf{L_1}$ (—) and [Pt($\mathbf{L_1}$)]$(SO_3CF_3)_2$ (—■—), and (c) $\mathbf{L_2}$ (—) and [Pt($\mathbf{L_2}$)]$(SO_3CF_3)_2$ (—■—).

plexation, relatively modest anodic shifts of 148 mV and 48 mV were observed for the first and second oxidations, respectively. Further, each oxidation is accompanied by a corresponding anodically shifted reduction wave. The modest shift in both redox couples along with their reversibility, as in the free ligand, suggests a much weaker interaction exists between the redox center in $\mathbf{L_2}$ and the captured platinum(II) ion. Of note, cyclic voltammograms of *p*-TMPD acquired in the presence of $[Pt(C_2H_5CN)_4](SO_3CF_3)_2$ showed no change in oxidation potential of the phenylenediamine moiety. We suggest then that the complex formed by $\mathbf{L_2}$ is primarily a thioether—Pt(II) chelation product, perhaps exocyclic, as has been reported for a number of metal—thiacrown ether complexes,[20] without direct bonding to the redox center. The S-bound complex draws the Pt(II) ion in close proximity to the redox center which then causes the anodic shift. A similar rationale has been used to describe the electrochemical response of a tetrathiafulvalene-containing crown ether to the barium cation.[21]

Conclusion

In summary, the Wurster's thiacrown ethers reported herein represent the first TMPD-based redox-active crowns targeting soft cationic guests. Two isomeric hosts were prepared using synthetic methods that have the ability to be generalized, and their solid-state structures were confirmed through single-crystal X-ray analysis. As anticipated, these ligands both display an affinity for Pt(II). The traditional crown architecture of $\mathbf{L_1}$ supports the formation of a Pt(II) complex that has strong interactions between the redox center and cationic guest, both in the solution and solid state. In the case of $\mathbf{L_2}$, a crownophane which presents the electron-rich π face of the phenylenediamine subunit as a possible ligating entity, a discrete Pt(II) complex was not isolated. However, electrochemical and spectroscopic data support complex formation, although it does not involve a strong interaction with the redox center.

Acknowledgment. This work was supported by the Robert A. Welch Foundation (Grant No. AT-1527).

Supporting Information Available: X-ray crystallographic data for $\mathbf{L_1}$, $\mathbf{L_2}$, and [Pt($\mathbf{L_1}$)]$(PF_6)_2$ in CIF format. This material is available free of charge via the Internet at http://pubs.acs.org.

IC051125D

(20) For examples, see: (a) Blake, A. J.; Reid, G.; Schröder, M. *J. Chem. Soc., Dalton Trans.* **1990**, 3849—3856. (b) Izatt, R. M.; Wu, G.; Jiang, W.; Dalley, N. K. *Inorg. Chem.* **1990**, *29*, 3828—3832. (c) Blake, A. J.; Reid, G.; Schröder, M. *J. Chem. Soc., Chem. Commun.* **1992**, 1074—1076.

(21) LeDerf, F.; Mazari, M.; Mercier, N.; Levillain, E.; Trippé, G.; Riou, A.; Richomme, P.; Becher, J.; Garín, J.; Orduna, J.; Gallego-Planas, N.; Gorgues, A.; Sallé, M. *Chem.—Eur. J.* **2001**, *7*, 447—455.